PHYSICAL REVIEW B **96**, 020412(R) (2017)

Quantum paramagnet and frustrated quantum criticality in a spin-one diamond lattice antiferromagnet

Gang Chen*

State Key Laboratory of Surface Physics, Department of Physics, Center for Field Theory & Particle Physics, Fudan University, Shanghai 200433, China

and Collaborative Innovation Center of Advanced Microstructures, Nanjing 210093, China

(Received 24 January 2017; published 21 July 2017)

Motivated by the proposal of a topological quantum paramagnet in the diamond lattice antiferromagnet $NiRh_2O_4$, we propose a minimal model to describe the magnetic interaction and properties of the diamond material with spin-one local moments. Our model includes the first- and second-neighbor Heisenberg interactions as well as a local single-ion spin anisotropy that is allowed by the spin-one nature of the local moment and the tetragonal symmetry of the system. We point out that there exists a quantum phase transition from a trivial quantum paramagnet when single-ion spin anisotropy is dominant to the magnetic ordered states when the exchange is dominant. Due to the frustrated spin interaction, the magnetic excitation in the quantum paramagnetic state supports extensively degenerate band minima in the spectra. As the system approaches the transition, extensively degenerate bosonic modes become critical at the criticality, giving rise to unusual magnetic properties. Our phase diagram and experimental predictions for different phases provide a guideline for the identification of the ground state for $NiRh_2O_4$. Although our results are fundamentally different from the proposal for topological quantum paramagnets, they represent interesting possibilities for spin-one diamond lattice antiferromagnets.

DOI: 10.1103/PhysRevB.96.020412

Introduction. The recent theoretical proposal of symmetry protected topological (SPT) ordered states has sparked wide interest in the theoretical community [1–25]. The well-known topological insulator, which was proposed and discovered earlier, is a noninteracting fermion SPT protected by time reversal symmetry [26,27]. In contrast, SPTs in bosonic systems must be stabilized by the interactions [11]. The spin degrees of freedom with exchange interactions seem to be a natural candidate for realizing boson SPTs [10]. In fact, the Haldane spin-one chain is a one-dimensional (1D) boson SPT and is protected by SO(3) spin rotational symmetry [1,2,28]. The realization of boson SPTs in high dimensions is still missing. It was suggested that a spin-one diamond lattice antiferromagnet with frustrated spin interactions may host a topological quantum paramagnet that is a spin analog of topological insulators and is protected by time reversal symmetry [29]. Quite recently, a diamond lattice antiferromagnet $NiRh_2O_4$ with Ni^{2+} spin-one local moments was proposed to fit into the early suggestion [30].

$NiRh_2O_4$ is a tetragonal spinel and experiences a structural phase transition from cubic to tetragonal at $T = 380$ K [30,32,33]. As we show in Fig. 1, the magnetic ion Ni^{2+} has a $3d^8$ electron configuration, forming a spin $S = 1$ local moment and occupying the tetrahedral diamond lattice site. No signature of magnetic order was observed down to 0.1 K in the magnetic susceptibility and specific heat measurements. Although this might fulfill the basic requirement for the absence of magnetic order in a topological quantum paramagnet, an alternative state that is distinct from topological quantum paramagnets may also provide a consistent experimental prediction with the current experiments. In this Rapid Communication, we propose a minimal spin model for a spin-one diamond lattice with tetragonal distortion and study the full phase diagram and phase transition of our model. We do not find the presence of a topological quantum paramagnet in our phase diagram. Instead, due to strong spin frustration, the ordered state in our phase diagram can be easily destabilized and converted into a trivial quantum paramagnet by moderate single-ion spin anisotropy. We predict that this seemingly trivial quantum paramagnetic state in a large parameter regime supports a gapped magnetic excitation that develops extensively degenerate band minima in the spectrum. As the quantum paramagnet approaches the phase transition to a proximate ordered state, the extensively degenerate low-energy modes become gapless and are responsible for unusual magnetic properties, such as a linear-T heat capacity at low temperatures in the vicinity of the transition. In the proximate

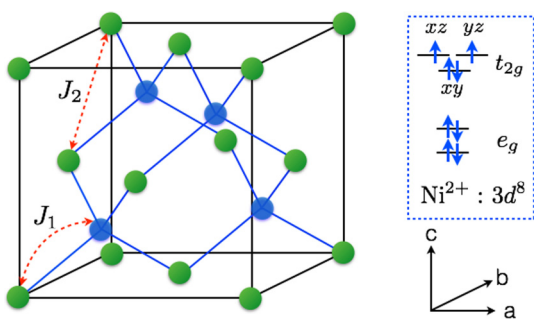

FIG. 1. A diamond lattice with J_1 and J_2 interactions. Due to the tetragonal symmetry of the lattice, the a and b directions are not equivalent to the c direction. The Ni^{2+} ion is in a tetrahedral environment, so the e_g orbitals are lower in energy than the t_{2g} levels. Tetragonal distortion further splits the two e_g orbitals and the three t_{2g} orbitals, but the degeneracy of the xz and yz orbitals remains intact under tetragonal distortion. To avoid the orbital degree of freedom, we here place the xz and yz orbitals above the xy orbitals [31].

*gangchen.physics@gmail.com

ordered phases, we further show that the spin spiral orders are actually induced by quantum fluctuations via quantum order by disorder.

The microscopic spin model. We here propose the following microscopic spin model that describes the interaction between the spin-1 local moments with the tetragonal symmetry,

$$H = J_1 \sum_{\langle rr' \rangle} \boldsymbol{S}_r \cdot \boldsymbol{S}_{r'} + J_2 \sum_{\langle\langle rr' \rangle\rangle} \boldsymbol{S}_r \cdot \boldsymbol{S}_{r'} + D_z \sum_r \left(S_r^z\right)^2, \quad (1)$$

where J_1 and J_2 are the first-neighbor and second-neighbor Heisenberg exchange interactions, respectively. Although the tetragonal lattice symmetry allows inequivalent bonds [33], in this minimal model we assume all bonds are equivalent. Since the diamond lattice is a bipartite lattice, the first-neighbor J_1 interaction alone is unfrustrated, and would favor a simple Néel state if J_1 is antiferromagnetic. The second-neighbor interaction J_2 is an interaction within each fcc sublattice of the diamond lattice. Due to the large numbers of second-neighbor bonds, the J_2 interaction would cause a spin frustration even when it is small compared to J_1. Moreover, additional single-ion spin anisotropy is further introduced on top of the spin exchange interactions, and is not included in the model in Ref. [33]. Spin anisotropy is naturally allowed by tetragonal lattice symmetry and is the only term occurring for a spin-one local moment such as the Ni^{2+} ion. Previous classical treatments of the J_1-J_2 spin model on a diamond lattice and the analysis of thermal fluctuation have led to the interesting discovery of a spiral spin liquid [34–37]. A quantum treatment of the J_1-J_2 model used an exotic SP(N) parton construction for the spins [38] and again worked in the ordered regime. In our context, we will largely treat spins and interactions quantum mechanically by a more conventional means that is appropriate for the J_1-J_2-D_z model.

Due to this single-ion spin anisotropy, the magnetic susceptibilities along different directions should reveal such spin anisotropy. In particular, we carry out a high-temperature series expansion and find that the Curie-Weiss temperatures for the magnetic field parallel and normal to the z direction are given as [31]

$$\Theta_{\rm CW}^{z} = -\frac{D_z}{3} - \frac{S(S+1)}{3}(z_1 J_1 + z_2 J_2), \quad (2)$$

$$\Theta_{\rm CW}^{\perp} = +\frac{D_z}{6} - \frac{S(S+1)}{3}(z_1 J_1 + z_2 J_2), \quad (3)$$

where $z_1 = 4$ and $z_2 = 12$ are the numbers of first-neighbor and second-neighbor bonds, respectively. The above prediction can be used to extract single-ion spin anisotropy. Note for a powder sample, the Curie-Weiss temperature is $\Theta_{\rm CW}^{\rm powder} = -\frac{S(S+1)}{3}(z_1 J_1 + z_2 J_2)$ and is thus independent of spin anisotropy.

Quantum paramagnet and phase diagram. To obtain a full phase diagram of the J_1-J_2-D_z model, we start from the parameter regime where single-ion spin anisotropy is dominant. We consider an easy-plane anisotropy with $D_z > 0$, since easy-axis spin anisotropy would stabilize the Néel state and enlarge its parameter regime. In the large and positive D_z limit, the ground state is a trivial quantum paramagnet with $S^z = 0$ on every site, $|\Psi\rangle = \prod_r |S_r^z = 0\rangle$. For this simple

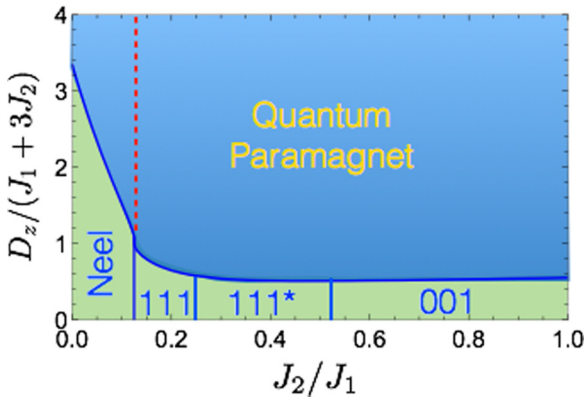

FIG. 2. The phase diagram of the J_1-J_2-D_z model. Because the powder sample Curie-Weiss temperature $\Theta_{\rm CW}^{\rm powder} = -8(J_1 + 3J_2)/3$, we set the energy unit of the spin anisotropy D_z to $J_1 + 3J_2$ in the plot. The transition from a quantum paramagnet to the ordered regions is continuous in mean-field theory. On the left of the (red) dashed line, the band minimum of the magnetic exciton is unique and appears at the Γ point. On the right side, the band minima form a degenerate surface in reciprocal space. Please refer to the main text for details.

state, there is no magnetic order and all the spin excitations are fully gapped. Since the global U(1) spin rotational symmetry around the z direction is preserved, the magnetic susceptibility at zero temperature for the field along the z direction is zero with $\chi_z(T = 0) = 0$. However, if the field is applied in the xy plane, spin rotational symmetry is broken by the in-plane field and the magnetic susceptibility is a constant with

$$\chi_\perp(T = 0) = \frac{2\mu_0(g\mu_{\rm B})^2}{D_z + 2(z_1 J_1 + z_2 J_2)}, \quad (4)$$

where g is the Landé factor. Again, this result is a consequence of single-ion anisotropy and can be used to detect the quantum paramagnetic state.

As we turn on the exchange interaction, the spin excitation would develop dispersion in momentum space. With a sufficient exchange interaction, we expect the minimum of the dispersion to touch the zero energy that would lead to magnetic orderings. To describe the magnetic ordering transition out of the quantum paramagnetic phase, we substitute the spin operators with rotor variables such that [39]

$$S_r^z = n_r, \quad S_r^{\pm} = \sqrt{2} e^{\pm i\phi_r}, \quad (5)$$

where ϕ_r is a 2π-periodic phase variable and n_r is integer valued. This substitution has enlarged the physical Hilbert space by allowing S^z or n to take values beyond 0 and ± 1. We, however, do not expect this approximation to cause significant effects since the nonphysical values of n_r have been energetically suppressed by large single-ion spin anisotropy. Moreover, the substitution preserves global U(1) spin rotational symmetry around the z direction of the original spin model. Finally, to preserve the spin commutation relation, we impose the commutation for ϕ_r and n_r with $[\phi_r, n_{r'}] = i\delta_{rr'}$.

With the rotor variables, the J_1-J_2-D_z spin model takes the form

$$H = \sum_{\langle \boldsymbol{r}\boldsymbol{r}'\rangle} J_1[2\cos(\phi_{\boldsymbol{r}} - \phi_{\boldsymbol{r}'}) + n_{\boldsymbol{r}} n_{\boldsymbol{r}'}] + \sum_{\langle\langle \boldsymbol{r}\boldsymbol{r}'\rangle\rangle} J_2[2\cos(\phi_{\boldsymbol{r}} - \phi_{\boldsymbol{r}'}) + n_{\boldsymbol{r}} n_{\boldsymbol{r}'}] + \sum_{\boldsymbol{r}} D_z n_{\boldsymbol{r}}^2. \quad (6)$$

From the symmetry point of view, the above model has the same symmetry as a standard boson Hubbard model, except it has an extra intersite boson interaction. To make this analogy a bit further, the quantum paramagnetic state is analogous to a boson Mott insulator with $n_{\boldsymbol{r}} = 0$ at every site, and the proximate magnetic order is as a superfluid of bosons. Despite the seeming similarity, we show below the intrinsic spin frustration brings a rather interesting dispersion of magnetic excitation in the quantum paramagnet and thus leads to unusual properties at the analogous "superfluid-Mott" transition [40].

The primary operators that are responsible for the magnetic transition out of the quantum paramagnet are the $S_{\boldsymbol{r}}^{\pm}$ spin operators that create the gapped spin excitations in the quantum paramagnet but take finite values in the ordered states. We here carry out a coherent state path integral and integrate out the number operator $n_{\boldsymbol{r}}$. The resulting partition function is

$$Z = \int \mathcal{D}\Phi_{\boldsymbol{r}} \mathcal{D}\lambda_{\boldsymbol{r}} \exp\left[-\mathcal{S} - i\sum_{\boldsymbol{r}} \lambda_{\boldsymbol{r}}(|\Phi_{\boldsymbol{r}}|^2 - 1)\right], \quad (7)$$

where the effective action for the rotor variable is

$$\mathcal{S} = \int d\tau \sum_{\boldsymbol{k}\in \mathrm{BZ}} (2D_z \mathbb{1}_{2\times 2} + \mathcal{J}_{\boldsymbol{k}})^{-1}_{ij} \partial_\tau \Phi^\dagger_{i,\boldsymbol{k}} \partial_\tau \Phi_{j,\boldsymbol{k}} + \sum_{\langle \boldsymbol{r}\boldsymbol{r}'\rangle} J_1 \Phi^\dagger_{\boldsymbol{r}} \Phi_{\boldsymbol{r}'} + \sum_{\langle\langle \boldsymbol{r}\boldsymbol{r}'\rangle\rangle} J_2 \Phi^\dagger_{\boldsymbol{r}} \Phi_{\boldsymbol{r}'}, \quad (8)$$

where we have introduced the variable $\Phi_{\boldsymbol{r}} \equiv e^{i\phi_{\boldsymbol{r}}}$. To impose the unimodular condition for $\Phi_{\boldsymbol{r}}$, we have introduced a Lagrange multiplier $\lambda_{\boldsymbol{r}}$ on each site to impose the unimodular condition $|\Phi_{\boldsymbol{r}}| = 1$ in Eq. (7). To solve for the dispersion of the excitation, we take a saddle-point approximation and choose a uniform mean-field ansatz such that $i\lambda_{\boldsymbol{r}} \equiv \beta\Delta(T)$, where $\beta = (k_B T)^{-1}$. We integrate out the $\Phi_{\boldsymbol{r}}$ field and obtain the saddle-point equation for $\Delta(T)$ in the quantum paramagnetic phase,

$$\sum_{i=1,2}\sum_{\boldsymbol{k}\in \mathrm{BZ}} \frac{2D_z + \xi_{i,\boldsymbol{k}}}{\omega_{i,\boldsymbol{k}}} \coth\left(\frac{\beta\omega_{i,\boldsymbol{k}}}{2}\right) = 2, \quad (9)$$

where $\omega_{1,\boldsymbol{k}}$ and $\omega_{2,\boldsymbol{k}}$ are the two modes of the magnetic excitations in the paramagnetic phase and are given by

$$\omega_{i,\boldsymbol{k}} = [(4D_z + 2\xi_{i,\boldsymbol{k}})(\Delta(T) + \xi_{i,\boldsymbol{k}})]^{\frac{1}{2}}, \quad (10)$$

and $\xi_{1,\boldsymbol{k}}$ and $\xi_{2,\boldsymbol{k}}$ are the two eigenvalues of the exchange matrix $\mathcal{J}_{\boldsymbol{k}}$ [31]. As one decreases single-ion spin anisotropy, the gap of the magnetic excitation decreases steadily. At the transition, the gap is closed and induces a magnetic order, and this phase transition is continuous within this treatment. In the phase diagram that is depicted in Fig. 2, the phase boundary between the quantum paramagnet and the magnetic order is then determined by examining the gap of the excitations in Eq. (10). In Fig. 2, the ordered region of the phase diagram is further split into several subregions with distinct magnetic orders from the quantum order by the disorder effect. This will be explained later.

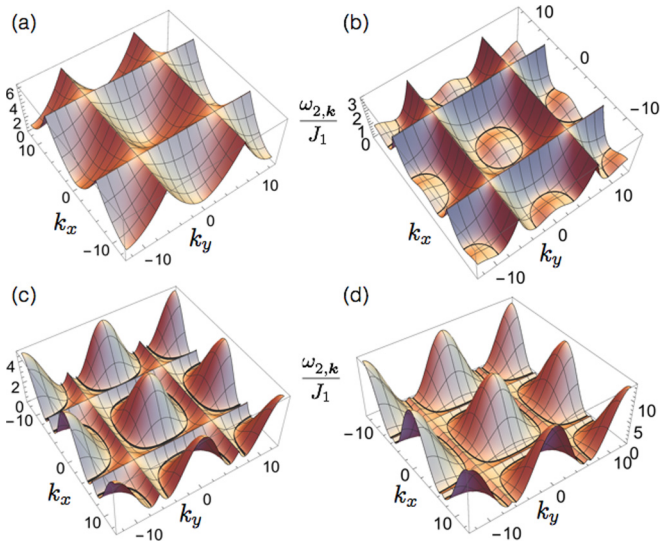

FIG. 3. The magnetic excitation $\omega_{2,\boldsymbol{k}}$ in the k_x-k_y plane of the quantum paramagnet. We have chosen the following parameters: (a) $J_2 = 0.05J_1, D_z = 3J_1$; (b) $J_2 = 0.18J_1, D_z = 1.5J_1$; (c) $J_2 = 0.4J_1$, $D_z = 1.5J_1$; (d) $J_2 = 0.8J_1$, $D_z = 2J_1$. In the figure, we set $k_z = 0$, and an extended zone with $k_x \in [-4\pi, 4\pi], k_y \in [-4\pi, 4\pi]$ is used. Degenerate minima are marked with contours. One can observe the evolution of the band minima.

Frustrated quantum criticality. Here, we point out nontrivial magnetic excitation in the quantum paramagnetic state and the resulting frustrated quantum criticality. When $J_2 < J_1/8$, the band minimum of the lower excitation $\omega_{2,\boldsymbol{k}}$ is at the Γ point. As we increase J_2 beyond $J_1/8$, the dispersion minima are obtained by minimizing $\xi_{2,\boldsymbol{k}}$. We find that the minima of $\omega_{2,\boldsymbol{k}}$ are extensively degenerate [41,42] and form a two-dimensional surface in three-dimensional reciprocal space that is defined by

$$\cos\frac{k_x}{2}\cos\frac{k_y}{2} + \cos\frac{k_x}{2}\cos\frac{k_z}{2} + \cos\frac{k_y}{2}\cos\frac{k_z}{2} = \frac{J_1^2}{16J_2^2} - 1, \quad (11)$$

where we have set the lattice constant to unity. This relation coincides with the degenerate spiral surface that was obtained in the classical treatment of the J_1-J_2 model [34,43]. In Fig. 3, we depict the band $\omega_{2,\boldsymbol{k}}$ in the k_x-k_y plane with $k_z = 0$.

Now we explain how the behaviors of the heat capacity in the vicinity of the magnetic critical point are modified by the large density of the low-energy excitations near the band minima. For $J_2 < J_1/8$, only a single bosonic mode becomes critical [see Fig. 3(a)] and leads to the usual $C_v \propto T^3$ up to a logarithmic correction from the quantum fluctuation at the criticality. For $J_2 > J_1/8$, however, a degenerate surface of bosonic modes becomes critical at the transition [see Figs. 3(b)–3(d)]. To understand the consequence of this unusual phenomena, we return to the saddle-point equation

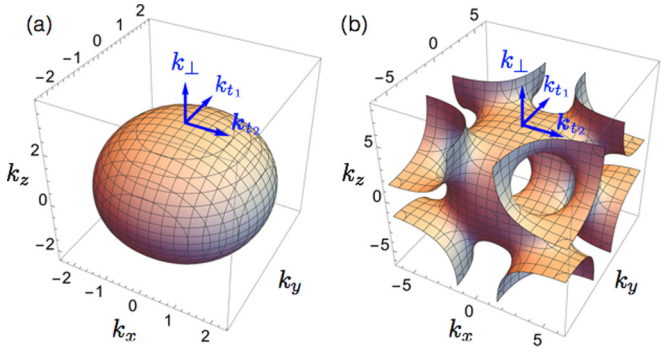

FIG. 4. The degenerate surface of the band minima at (a) $J_2 = 0.18J_1$ and (b) $J_2 = J_1/3$. The (k_{t_1}, k_{t_2}) are the two tangential momenta and $k_\perp$ is the component normal to the degenerate surface.

in Eq. (9) that reduces to

$$A\int_0^\Lambda dk_\perp \int_\Sigma d^2\boldsymbol{k}_t \frac{\coth\left[\frac{\beta}{2}(m^2+v^2k_\perp^2)^{\frac{1}{2}}\right]}{(m^2+v^2k_\perp^2)^{\frac{1}{2}}} + c = 2, \quad (12)$$

where we have singled out the contribution from the critical modes as the first term in Eq. (12), A is an unimportant prefactor of the integration, and c is an approximately T-independent contribution from the remaining part of the excitations. In Eq. (12), we have chosen the coordinate basis $(\boldsymbol{k}_t, k_\perp)$ such that $\boldsymbol{k}_t$ $(k_\perp)$ refer to the components of the momentum tangential to (normal to) the degenerate surface Σ (see Fig. 4), and Λ is the momentum cutoff. Here, the critical mode behaves as $\omega_{2,\boldsymbol{k}} \simeq (m^2+v^2k_\perp^2)^{\frac{1}{2}}$ in which m is the thermally generated mass term and v is the velocity normal to the degenerate surface. At low temperatures ($T \ll \Lambda$), the temperature-dependent part of the integral becomes independent of the cutoff Λ, and only depends on T via the dimensionless parameter m^2/T^2. In order for the equality in Eq. (12) to hold, we expect $m \propto T$.

From the scaling form of m, we obtain a remarkable result for the low-temperature heat capacity that behaves as $C_v \propto T$ at the criticality. This linear-T heat capacity is similar to the one in a Fermi-liquid metal, except that this is a pure bosonic system. This unusual behavior simply arises from the frustrated spin interaction.

Quantum order by disorder. When extensively degenerate modes are condensed at the critical point for $J_2 > J_1/8$, extensively degenerate candidate ordered states are available, and it is the quantum fluctuation of the spins that selects the particular orders in the phase diagram of Fig. 2.

To explain this phenomenon, we first realize that easy-plane spin anisotropy favors the magnetic order in the xy plane with

$$\boldsymbol{r} \in \mathrm{A}, \quad \boldsymbol{S}_{\boldsymbol{r}} = S\,\mathrm{Re}[(\hat{x} - i\hat{y})e^{i\boldsymbol{q}\cdot\boldsymbol{r}}], \quad (13)$$

$$\boldsymbol{r} \in \mathrm{B}, \quad \boldsymbol{S}_{\boldsymbol{r}} = S\,\mathrm{Re}[(\hat{x} - i\hat{y})e^{i\boldsymbol{q}\cdot\boldsymbol{r}+i\theta_{\boldsymbol{q}}}], \quad (14)$$

where $\boldsymbol{q}$ is the propagating wave vector of the spin spiral, and $\theta_{\boldsymbol{q}}$ is the phase shift between the A and B sublattices of the diamond lattice. Both $\boldsymbol{q}$ and $\theta_{\boldsymbol{q}}$ can be obtained by a Weiss mean-field theory that is similar to the early classical treatment [34]. The quantum fluctuation with respect to the candidate spin spiral state is analyzed by a linear spin-wave theory and is discussed in detail in the Supplemental Material [31]. As we plot in Fig. 2, quantum fluctuation favors the spiral wave vector to be either along the [001] or [111] direction. For $J_2 > J_1/4$, the degenerate surface has expanded to the Brillouin zone boundary, and the [111] direction no longer intersects with the degenerate surface [see Fig. 4(b) as an example], the six points around the [111] direction are selected, and the resulting ordering states are labeled by [111*] in Fig. 2.

Discussion. Contrary to the proposal of a topological quantum paramagnet in $NiRh_2O_4$ [30], our theoretical prediction does not support a topological quantum paramagnet in our minimal J_1-J_2-D_z spin model. Instead, due to the strong frustrated spin interaction, a large region of the trivial quantum paramagnet state is stabilized in the phase diagram. Although the trivial quantum paramagnet does not represent any new state of matter, the magnetic excitation is rather unusual and supports a degenerate surface of band minima in the spectrum. As the system is driven into a magnetic ordered state, extensively degenerate critical modes from the degenerate surface are condensed, leading to unconventional critical properties at the transition.

To differentiate the proposal of a topological quantum paramagnet from our proposal, we propose the following experiments. In a topological quantum paramagnet, the bulk is fully gapped and the surface may show various anomalous behaviors [7,11,23,29]. If the system develops gapless surface states, it should be detectable by surface thermal transport. If the system realizes intrinsic topological order [7,23], one would observe fractionalized excitations on the surface. If the system breaks time reversal symmetry on the surface, then one would observe a surface magnetic order. In contrast, our prediction of the thermodynamic properties and the excitation spectrum for a trivial quantum paramagnet can be directly measured by bulk measurements, such as magnetic susceptibility and inelastic neutron scattering. Moreover, since the model is applicable broadly to spin-one tetragonal diamond materials, it is of interest to find similar materials in the spinel families.

Finally, we address the role of other interactions. It has been shown classically for the spin $S = 5/2$ diamond lattice antiferromagnet $MnSc_2S_4$ that a very weak third-neighbor interaction could lift the continuous degeneracy [34]. Here, the quantum paramagnetic phase is a robust state, the presence of a weak further neighbor interaction cannot destabilize it, and we expect the general structure of the phase diagram in Fig. 2 to remain intact. The effect of other weak interactions on the excitation in quantum paramagnets is a very-low-energy scale property and may not be visible under the current experimental resolution.

Note added. Recently, we became aware of Ref. [44], which studied a modified exchange model for $NiRh_2O_4$. Their results are complementary to ours.

Acknowledgments. We acknowledge an anonymous referee for criticism and comments that helped improve the paper. This work is supported by the Ministry of Science and Technology of China with Grant No. 2016YFA0301001, the Start-Up Funds and the Program of First-Class University Construction

of Fudan University, and the Thousand-Youth-Talent Program of China. I thank Prof. Nanlin Wang for hospitality during my visit to ICQM of Peking University, Prof. Zhong Wang for hospitality during my visit to IAS of Tsinghua University, Prof. Chen Fang for hospitality during my visit to IOP, and Prof. Ying Ran for hospitality during my visit to Boston College when this work was motivated and finalized. I thank Prof. Yang Qi and Dr. Peng Ye for a conversation that pointed to other surface possibilities that are consistent with Prof. T. Senthil's later comments. Finally, I thank Prof. T. McQueen and Prof. Senthil for recent correspondence and comments.

[1] Z.-C. Gu and X.-G. Wen, Tensor-entanglement-filtering renormalization approach and symmetry-protected topological order, Phys. Rev. B **80**, 155131 (2009).

[2] F. Pollmann, A. M. Turner, E. Berg, and M. Oshikawa, Entanglement spectrum of a topological phase in one dimension, Phys. Rev. B **81**, 064439 (2010).

[3] X. Chen, Z.-C. Gu, and X.-G. Wen, Classification of gapped symmetric phases in one-dimensional spin systems, Phys. Rev. B **83**, 035107 (2011).

[4] F. Pollmann, E. Berg, A. M. Turner, and M. Oshikawa, Symmetry protection of topological phases in one-dimensional quantum spin systems, Phys. Rev. B **85**, 075125 (2012).

[5] X. Chen, Z.-C. Gu, Z.-X. Liu, and X.-G. Wen, Symmetry protected topological orders and the group cohomology of their symmetry group, Phys. Rev. B **87**, 155114 (2013).

[6] T. Senthil, Symmetry-protected topological phases of quantum matter, Annu. Rev. Condens. Matter Phys. **6**, 299 (2015).

[7] A. Vishwanath and T. Senthil, Physics of Three-Dimensional Bosonic Topological Insulators: Surface-Deconfined Criticality and Quantized Magnetoelectric Effect, Phys. Rev. X **3**, 011016 (2013).

[8] C. Xu and T. Senthil, Wave functions of bosonic symmetry protected topological phases, Phys. Rev. B **87**, 174412 (2013).

[9] C. Wang and T. Senthil, Boson topological insulators: A window into highly entangled quantum phases, Phys. Rev. B **87**, 235122 (2013).

[10] X. Chen, Z.-C. Gu, and X.-G. Wen, Complete classification of one-dimensional gapped quantum phases in interacting spin systems, Phys. Rev. B **84**, 235128 (2011).

[11] X. Chen, Z.-C. Gu, Z.-X. Liu, and X.-G. Wen, Symmetry-protected topological orders in interacting bosonic systems, Science **338**, 1604 (2012).

[12] H. Song, Sh.-J. Huang, L. Fu, and M. Hermele, Topological Phases Protected by Point Group Symmetry, Phys. Rev. X **7**, 011020 (2017).

[13] M. A. Metlitski, C. L. Kane, and M. P. A. Fisher, Bosonic topological insulator in three dimensions and the statistical Witten effect, Phys. Rev. B **88**, 035131 (2013).

[14] M. A. Metlitski, C. L. Kane, and M. P. A. Fisher, Symmetry-respecting topologically ordered surface phase of three-dimensional electron topological insulators, Phys. Rev. B **92**, 125111 (2015).

[15] Y.-M. Lu and A. Vishwanath, Theory and classification of interacting integer topological phases in two dimensions: A Chern-Simons approach, Phys. Rev. B **86**, 125119 (2012).

[16] X. Chen, Y.-M. Lu, and A. Vishwanath, Symmetry-protected topological phases from decorated domain walls, Nat. Commun. **5**, 3507 (2014).

[17] Z. Bi, A. Rasmussen, K. Slagle, and C. Xu, Classification and description of bosonic symmetry protected topological phases with semiclassical nonlinear sigma models, Phys. Rev. B **91**, 134404 (2015).

[18] Z. Bi and C. Xu, Construction and field theory of bosonic-symmetry-protected topological states beyond group cohomology, Phys. Rev. B **91**, 184404 (2015).

[19] M. Hermele and X. Chen, Flux-Fusion Anomaly Test and Bosonic Topological Crystalline Insulators, Phys. Rev. X **6**, 041006 (2016).

[20] S. D. Geraedts and O. I. Motrunich, Model Realization and Numerical Studies of a Three-Dimensional Bosonic Topological Insulator and Symmetry-Enriched Topological Phases, Phys. Rev. X **4**, 041049 (2014).

[21] S. D. Geraedts and O. I. Motrunich, Exact models for symmetry-protected topological phases in one dimension, arXiv:1410.1580.

[22] P. Ye and Z.-C. Gu, Topological quantum field theory of three-dimensional bosonic Abelian-symmetry-protected topological phases, Phys. Rev. B **93**, 205157 (2016).

[23] P. Ye and Z.-C. Gu, Vortex-Line Condensation in Three Dimensions: A Physical Mechanism for Bosonic Topological Insulators, Phys. Rev. X **5**, 021029 (2015).

[24] P. Ye and X.-G. Wen, Projective construction of two-dimensional symmetry-protected topological phases with U(1), SO(3), or SU(2) symmetries, Phys. Rev. B **87**, 195128 (2013).

[25] P. Ye and X.-G. Wen, Constructing symmetric topological phases of bosons in three dimensions via fermionic projective construction and dyon condensation, Phys. Rev. B **89**, 045127 (2014).

[26] M. Z. Hasan and C. L. Kane, Colloquium: Topological insulators, Rev. Mod. Phys. **82**, 3045 (2010).

[27] X.-L. Qi and S.-C. Zhang, Topological insulators and superconductors, Rev. Mod. Phys. **83**, 1057 (2011).

[28] F. D. M. Haldane, Continuum dynamics of the 1-D Heisenberg antiferromagnet: Identification with the O(3) nonlinear sigma model, Phys. Lett. A **93**, 464 (1983).

[29] C. Wang, A. Nahum, and T. Senthil, Topological paramagnetism in frustrated spin-1 Mott insulators, Phys. Rev. B **91**, 195131 (2015).

[30] J. Chamorro and T. McQueen, $S = 1$ on a Diamond Lattice in $NiRh_2O_4$, APS March Meeting Abstract **B48.00006**, 2017.

[31] See Supplemental Material at http://link.aps.org/supplemental/10.1103/PhysRevB.96.020412 for a detailed discussion.

[32] S. Horiuti and S. Miyahara, Tetragonal distortion of $NiRh_2O_4$, J. Phys. Soc. Jpn. **19**, 423 (1964).

[33] J. R. Chamorro and T. M. McQueen, Frustrated $S = 1$ on a Diamond Lattice, arXiv:1701.06674.

[34] D. Bergman, J. Alicea, E. Gull, S. Trebst, and L. Balents, Order-by-disorder and spiral spin-liquid in frustrated diamond-lattice antiferromagnets, Nat. Phys. **3**, 487 (2007).

[35] S. Gao, O. Zaharko, V. Tsurkan, Y. Su, J. S. White, G. S. Tucker, B. Roessli, F. Bourdarot, R. Sibille, D. Chernyshov *et al.*, Spiral spin-liquid and the emergence of a vortex-like state in $MnSc_2S_4$, Nat. Phys. **13**, 157 (2016).

[36] S. B. Lee and L. Balents, Theory of the ordered phase in *a*-site antiferromagnetic spinels, Phys. Rev. B **78**, 144417 (2008).

[37] L. Savary, E. Gull, S. Trebst, J. Alicea, D. Bergman, and L. Balents, Impurity effects in highly frustrated diamond-lattice antiferromagnets, Phys. Rev. B **84**, 064438 (2011).

[38] J.-S. Bernier, M. J. Lawler, and Y. B. Kim, Quantum Order by Disorder in Frustrated Diamond Lattice Antiferromagnets, Phys. Rev. Lett. **101**, 047201 (2008).

[39] G. Chen, M. Hermele, and L. Radzihovsky, Frustrated Quantum Critical Theory of Putative Spin-Liquid Phenomenology in 6*H*-B-$Ba_3NiSb_2O_9$, Phys. Rev. Lett. **109**, 016402 (2012).

[40] M. P. A. Fisher, P. B. Weichman, G. Grinstein, and D. S. Fisher, Boson localization and the superfluid-insulator transition, Phys. Rev. B **40**, 546 (1989).

[41] T. A. Sedrakyan, L. I. Glazman, and A. Kamenev, Absence of Bose condensation on lattices with moat bands, Phys. Rev. B **89**, 201112 (2014).

[42] T. A. Sedrakyan, L. I. Glazman, and A. Kamenev, Spontaneous Formation of a Nonuniform Chiral Spin Liquid in a Moat-Band Lattice, Phys. Rev. Lett. **114**, 037203 (2015).

[43] J. Attig and S. Trebst, Classical spin spirals in frustrated magnets from free-fermion band topology, arXiv:1705.04073.

[44] F. L. Buessen, M. Hering, J. Reuther, and S. Trebst, Quantum spin liquids in frustrated spin-1 diamond antiferromagnets, arXiv:1706.06299.